PCCP

PAPER

Cite this: *Phys. Chem. Chem. Phys.*, 2018, **20**, 7508

A computational study of supported Cu-based bimetallic nanoclusters for CO oxidation

Yulu Liu,†[ab] Hao Li,†[b] Wanglai Cen,[bc] Jianjun Li,*[a] Zhengming Wang[d] and Graeme Henkelman*[b]

Received 22nd December 2017,
Accepted 8th February 2018

DOI: 10.1039/c7cp08578h

rsc.li/pccp

In this study, we used DFT calculations to investigate the bi-functional nature of Cu-based alloy nanoclusters (NCs) supported on CeO_2(111) for CO oxidation. More specifically, we studied the reaction pathways on Cu_3Pt_7 and Cu_3Rh_7 *via* the O_2 associative (OCOO) and dissociative mechanisms. We find that CO oxidation on Cu_3Pt_7 proceeds *via* the O_2 dissociation pathway, while Cu_3Rh_7 prefers the OCOO mechanism. Combined with our previous results on Cu_3Au_7, we find that bi-functional CO oxidation on Cu-based alloys follows a Brønsted–Evans–Polanyi relationship, which provides a useful metric for the design of bi-functional alloyed catalysts.

1. Introduction

The toxic nature of carbon monoxide (CO), which is produced in large quantities by the petrochemical industry, has prompted research into strategies for CO oxidation at low temperature.[1] Catalytic oxidation of CO is being investigated not only because of its importance in environmental fields, but also as a prototypical reaction for heterogeneous catalysis.[2] Due to its prominent oxygen storage and release capacity and unique electronic properties regarding the highly localized 4f orbital, CeO_2 has been widely used as a supporting material in heterogeneous catalysis.[3–6] Since Haruta's pioneering study on the exceptionable catalytic activity of CO oxidation over the oxide-supported Au nanoparticles (NPs),[7] CeO_2-supported Au has been the subject of many experimental and theoretical studies.[4,8–11] In the work reported by Kim *et al.*,[4] focusing on CO oxidation over CeO_2-supported Au nanoclusters (NCs), it was found that CO has a strong binding as compared with O_2, which would lead to surface poisoning with CO and a low oxidation rate. Roldan *et al.*[12] studied O_2 adsorption and dissociation on Au_n (n = 5–79) clusters and found that O_2 has a low binding energy and a high dissociation barrier on Au NCs. In addition to Au, studies on many other monometallic catalysts for CO oxidation have been reported, such as Pd,[13–15] Ag,[16,17] Pt,[18–20] Rh,[21,22] and Cu.[16,23–25]

Alloyed catalysts, and especially alloyed metallic NPs, have also attracted much attention in recent years. Due to the synergetic influences of atomic ensemble, electronic and strain effects, alloyed systems have shown significantly enhanced catalytic activities compared to their monometallic counterparts.[26–29] Cu, a common transition metal in nature, has a strong oxygen affinity at room temperature[30,31] and has been widely considered as an alloying element in experimental[23,32,33] and theoretical studies[34,35] for CO oxidation. Luo *et al.*[36] found that a small amount of Cu can dramatically increase the activity of CO oxidation on Pt NPs. Liu *et al.*[23] also reported that only a small percentage of Cu was sufficient to promote the catalytic activity of CeO_2 by several orders of magnitude, while excessive amounts of Cu were detrimental for the thermal and hydrothermal stability of the catalyst. Zhang *et al.*[37] found that Au_7Cu_3 NCs supported on CeO_2(111) could separate the adsorption sites for CO and O_2, having a "bi-functional" effect for CO oxidation. They concluded that the Au–Cu interface provides an active site for CO oxidation, having a relatively low activation barrier. For other reactions, bi-functional effects at the alloyed interface sites also have shown excellent selectivity and activity, including the Pd–Au sites for formic acid decomposition[38] and ethanol dehydrogenation.[39,40]

Here we chose Cu as the oxophilic base and considered a set of alloying transition metals in the form of Cu_3X_7/CeO_2(111) (X = Pt, Rh, Ag, Ru, Zn, Co, Fe and Pd); these bimetallic NCs were screened for bi-functional CO oxidation capabilities. More specifically, we selected Cu_3Pt_7 and Cu_3Rh_7 as examples for mechanistic studies of CO oxidation, using density functional theory calculations (DFT) corrected by on-site coulomb interactions (DFT+U). Through these calculations, we found a

[a] *College of Architecture and Environment, Sichuan University, P. R. China. E-mail: jjli@scu.edu.cn*
[b] *Department of Chemistry and the Institute for Computational Engineering and Sciences, The University of Texas at Austin, 100 East 24th Street, Stop A1590, Austin, Texas 78712, USA. E-mail: henkelman@utexas.edu*
[c] *Institute of New Energy and Low Carbon Technology, Sichuan University, P. R. China*
[d] *Environmental Management Research Institute, National Institute of Advanced Industrial Science and Technology, 16-1 Onogawa, Tsukuba, Ibaraki 305-5869, Japan*
† These authors contributed equally to this work.

Brønsted–Evans–Polanyi (BEP) relationship for Cu_3Pt_7, Cu_3Rh_7 and Cu_3Au_7[37] as catalysts for CO oxidation. This scaling relation for the activation barrier of CO bi-functional oxidation of NCs provides guidance for the rational design of alloy catalysts.

2. Computational methods

DFT+U calculations were performed using the Vienna ab initio simulation package (VASP).[41,42] To model the highly localized Ce 4f orbital, we conducted spin-polarized DFT+U[43] with U_{eff} = 5 eV.[4,37,44,45] Core-valence interactions were described within the projector-augmented wave framework.[46] A plane wave basis with an energy cutoff of 400 eV was used to describe the valence electrons. The generalized gradient approximation using the Perdew–Burke–Ernzerhof functional was used to model electronic exchange and correlation.[47] A Gaussian smearing with a width of 0.05 eV was used to improve the convergence of states near the Fermi level. The Brillouin zone was sampled at the Gamma point. Convergence criterion for the electronic structure and the atomic geometry was 10^{-4} eV and 0.05 eV Å^{-1}, respectively. Transition states (TSs) for the CO oxidation reactions were located with the climbing-image nudged elastic band (cNEB) method.[48,49] Activation energies (E_a) were calculated as the energy difference between the transition and initial states. The binding energies E_b were defined as:

$$E_b = E_{molecule*} - E_{molecule} - E_*, \quad (1)$$

where $E_{molecule*}$ is the total energy of the system with the adsorbed molecule; $E_{molecule}$ and E_* are the energies of the gas phase molecule (in a vacuum) and the bare site, respectively. A negative binding energy indicates exothermic adsorption.

Compared to CeO_2(110) and (100), CeO_2(111) is thermodynamically favorable and thus is the most common catalytic support experimentally.[50–53] Accordingly, in this study, a 4 × 4 CeO_2(111) slab model with six atomic layers and 12 Å of vacuum was modeled to describe the CeO_2 support. For geometry optimization, atoms in the bottom three atomic layers were kept fixed at their bulk positions; all other atoms were free to relax. Similar to our previous study,[37] we used a symmetric hexagonal two-layered NCs composed of ten atoms (Cu_3X_7, where X represents other transition metals) supported on the CeO_2(111) surfaces (Fig. 1a). The model of Cu_3X_7/CeO_2(111) is derived from the hcp-like Au_{10} structure on CeO_2, which is found to be one of the most stable geometries on CeO_2.[4,54]

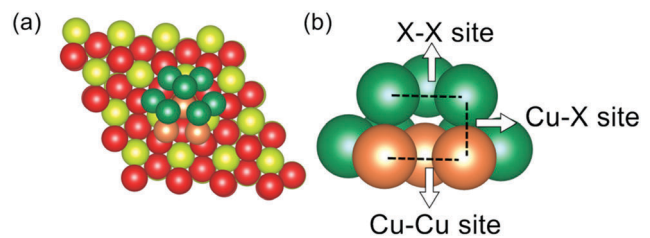

Fig. 1 (a) Cu_3X_7 clusters supported on the CeO_2(111) surface; (b) binding sites for O_2 and CO. Red, yellow, orange and green spheres represent O, Ce, Cu and X atoms.

While we can guarantee that this will be the most stable structure, especially under reaction conditions, we do know that such small bimetallic clusters will necessarily have the interface sites that we are studying in terms of the bifunctional catalytic properties. Additionally, both theoretical and experimental studies[24,55] have shown that even some bimetallic metastable structures can give rise to high catalytic activity at the bimetallic interface. With this model, there are three catalytic sites for CO oxidation: X–X, Cu–X interface and Cu–Cu sites (see Fig. 1b).

3. Results and discussion

3.1 Binding sites of O_2 and CO

Table 1 shows the calculated binding energies of O_2 and CO adsorbed at the Cu–X, Cu–Cu and X–X sites (the latter two include the atop and bridge sites of Cu or X atoms). Most of the tested Cu_3X_7 NCs are able to separate the binding sites for O_2 and CO, meaning that the two molecules favor binding to different sites. The exceptions are Cu_3Ru_7 which favors oxygen binding and Cu_3Pd_7 which favors CO binding. In both cases, the high coverage of a single specie will hinder CO oxidation. For Cu_3Pt_7, Cu_3Rh_7, Cu_3Co_7 and Cu_3Fe_7, the Cu sites are oxophilic and the X sites favor CO adsorption. However, for Cu_3Ag_7 and Cu_3Zn_7, the X sites prefer O_2 binding while the Cu sites favor CO adsorption. In these 'separable' systems, O_2 and CO do not compete for binding sites and are candidates for bi-functional CO oxidation.

As a case study, we chose Cu_3Pt_7 and Cu_3Rh_7 for an analysis of the CO bi-functional oxidation mechanism because they respectively represent two different types of miscibilities: CuPt is miscible in bulk, while CuRh is immiscible. Though CuRh is classically immiscible, there are some state-of-the-art methods (*e.g.*, microwave-assisted synthesis)[56] that have successfully been used to make immiscible Rh-based catalysts, including RhAu,[55] RhAg[29,57] and RhPd.[58] For both CuPt and CuRh, we have tested co-adsorption structures of CO and O_2. Although O_2 adsorption is not favorable on the Cu–X site of Cu_3Pt_7 or the Cu–Cu site of Cu_3Rh_7 (Table 1), O_2 adsorption on these sites becomes favorable when CO is coadsorbed, as shown in the optimized structures of the Cu_3Pt_7 system in Fig. 2a and c. As for Cu_3Rh_7, when O_2 is adsorbed on the Cu–Cu site in the

Table 1 Calculated binding energies (E_b, eV) of O_2 and CO at the binding sites of Cu–X/CeO_2 (X = Pt, Rh, Ag, Ru, Zn, Co, Fe and Pd) catalysts[a]

		Pt	Rh	Ag	Ru	Zn	Co	Fe	Pd
Cu–X	O_2	—	−1.68	−1.06	−2.21	−1.18	−1.84	—	−1.74
	CO	−1.28	—	—	—	−1.28	—	−2.10	−1.85
Cu–Cu	O_2	−0.78	—	—	−0.5	−0.42	—	−0.80	—
	CO	−0.54	—	−1.01	—	−1.29	−0.18	—	—
X–X	O_2	−1.92	−2.14	−0.91	−2.30	−1.53	—	—	−1.05
	CO	−2.35	−2.25	−0.59	−2.17	−1.14	−1.58	−1.38	−1.56

[a] Missing entries either do not provide stable binding sites or have a large structural distortion after relaxation.

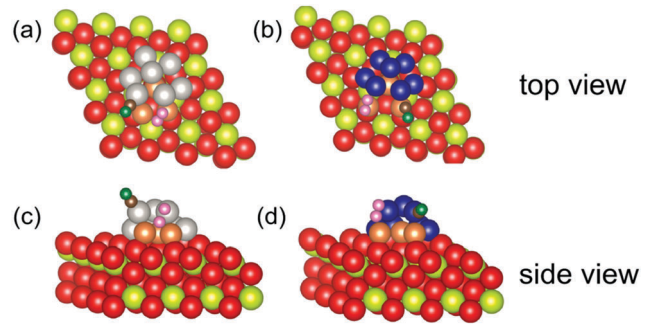

Fig. 2 Top views (a and b) and side views (c and d) of CO and O_2 adsorption on the Cu_3Pt_7/CeO_2 and Cu_3Rh_7/CeO_2 surfaces. Red, yellow, orange, silver, blue, pink, grey and green spheres represent oxygen (in ceria), Ce, Cu, Pt, Rh, oxygen (in the gas phase), carbon and oxygen atoms (from CO), respectively.

presence of adsorbed CO, there is a low diffusion barrier (*ca.* 0.1 eV) for O_2 diffusion from the Cu–Cu site to the Cu–X site. Therefore, we do not consider O_2 adsorption on the Cu–Cu site of Cu_3Rh_7 in this study. For clarity and for a direct comparison, we consider O_2 adsorption at the interface, namely the Cu–X sites of the two systems (Fig. 2), which are used for the subsequent O_2 associative mechanism that forms the O–C–O–O transition state for CO oxidation.

3.2 OCOO mechanisms

Fig. 3a and b show the OCOO mechanism for CO oxidation on Cu_3Pt_7 and Cu_3Rh_7. At the 1st CO oxidation stage ($CO + O_2 + * \rightarrow O–C–O–O^*$ (TS) $\rightarrow CO_2 + O^*$), Cu_3Rh_7 has a lower activation energy (0.70 eV) than that of Cu_3Pt_7 (1.23 eV). The two partial pathways are exothermic and thermodynamically feasible. The 2nd CO oxidation with the residual O atom on Cu_3Pt_7 and Cu_3Rh_7 ($CO + O^* \rightarrow CO_2 + *$) is shown in Fig. 3. Cu_3Pt_7 has an activation energy of 0.5 eV, which is lower than that of Cu_3Rh_7 (E_a = 0.84 eV, as shown in Fig. 3b). It should be noted that the reaction pathway on Cu_3Pt_7 is exothermic, while that on Cu_3Rh_7 is endothermic, requiring 0.59 eV.

Fig. 3c shows the corresponding pathways on Cu_3Au_7, as reported by Zhang *et al.*[37] It can be seen that Cu_3Au_7 has the lowest CO oxidation barriers (0.11 eV for the initial pathway; 0.23 eV for the subsequent pathway), compared to Cu_3Pt_7 and Cu_3Rh_7. Based on the pathways calculated from the three Cu-based models, we find a correlation between the activation energy (E_a) and reaction energy (E_r) that follows a BEP relationship (Fig. 4). R^2 of the linear relationship for the initial pathway is 0.89 which should be sufficient to predict the barrier of CO oxidation in other Cu-based bimetallic catalysts, including those shown in Table 1. R^2 of the subsequent CO oxidation is 0.99, which should reliably predict CO oxidation with the residual O atom in other Cu-based catalysts.

3.3 O_2 dissociative mechanisms

When O_2 is adsorbed at the Cu–Cu sites on Cu_3Pt_7, we found an alternative pathway for CO oxidation through the O_2 dissociative mechanism (Fig. 5). Firstly, O_2 dissociates into two O adatoms, where one O adsorbs on the Cu–Cu bridge site and the other at the Cu–X site. This process has a rather low activation energy (0.16 eV), which is thermodynamically and kinetically feasible. Then, CO adsorbed on the Pt–Pt bridge site reacts with the O atom on the interface of the Cu–Pt site with an activation energy of 1.04 eV, which is lower than that of the OCOO mechanism (1.23 eV). The last step that the 2nd CO connecting with the residual O atom is the same as that of the OCOO mechanism. It can be seen that the CO and O_2 co-adsorption energy (Fig. 5) is lower than that shown in Fig. 3a. Therefore, we expect that a stable co-adsorption structure would lead to a lower activation energy.

Shin *et al.*[59] also studied Pt@Cu NPs for CO oxidation. They found that exposed portions of the Pt core preferentially bind CO while the Cu shell binds O_2, and that CO oxidation will proceed at the Pt–Cu interface sites that are not poisoned by either CO or O_2. In addition, the Cu(111) and Cu(110) surfaces rapidly activate O_2 into dissociated O atoms with small barriers of 0.01 eV and 0.16 eV, respectively. The latter barrier is the same as that of the Cu_3Pt_7 model. Interestingly, the barriers for the next step, CO_2 formation, are 1.04 eV and 0.66 eV, respectively on Cu(111) and Cu(110), the former being similar to the CO_2 formation step in our model. This prior work provides confidence that our model is reasonable for a general description of bi-functional CO oxidation at interface sites.

As for Cu_3Rh_7 (which is shown in Fig. 2b), after O_2 dissociation, the process of CO association with O atoms is highly endothermic, with a reaction energy of 0.99 eV. Therefore, it is expected that the activation energy of this process would exceed 1.00 eV, which is significantly higher than that of the OCOO mechanism (0.70 eV) on Cu_3Rh_7. Thus, we do not expect that the O_2 dissociative mechanism on Cu_3Rh_7 is favorable.

3.4 Discussion

Our calculations show that O_2 adsorption on the interface site (Cu–X) tends to proceed the associative (OCOO) pathway, while O_2 adsorption on the Cu–Cu site prefers the dissociative pathway. A possible explanation is that different adsorption sites (the pure metal surface and alloy interface) on the catalysts have different local density of states due to d-band mixing *via* alloying,[40] which leads to different adsorption modes and reaction pathways. The Cu–Au system, from Zhang's previous report,[37] favored CO oxidation *via* an OCOO pathway on Cu–Cu and Cu–Au sites. The difference is that Au is relatively inert and is unable to activate the O_2 molecule, leaving only the OCOO pathway. However, Pt is able to activate O_2 so that the Cu–Pt system prefers the O_2 dissociation pathway.

A Bader charge analysis[60] shows that Cu atoms are positively charged and thus slightly oxidized, which is consistent with previous theoretical studies.[59] Under CO oxidation conditions, where the O_2 partial pressure is generally greater than CO, we believe that Cu and other oxophilic metals should be partially oxidized. Interestingly, Cu^+ ions are also found to be reactive for CO oxidation,[59,61–63] which could then form a mixed oxide with the oxide support. It is also possible that O near the Cu–X boundary will participate in rapid CO oxidation, as we suggest

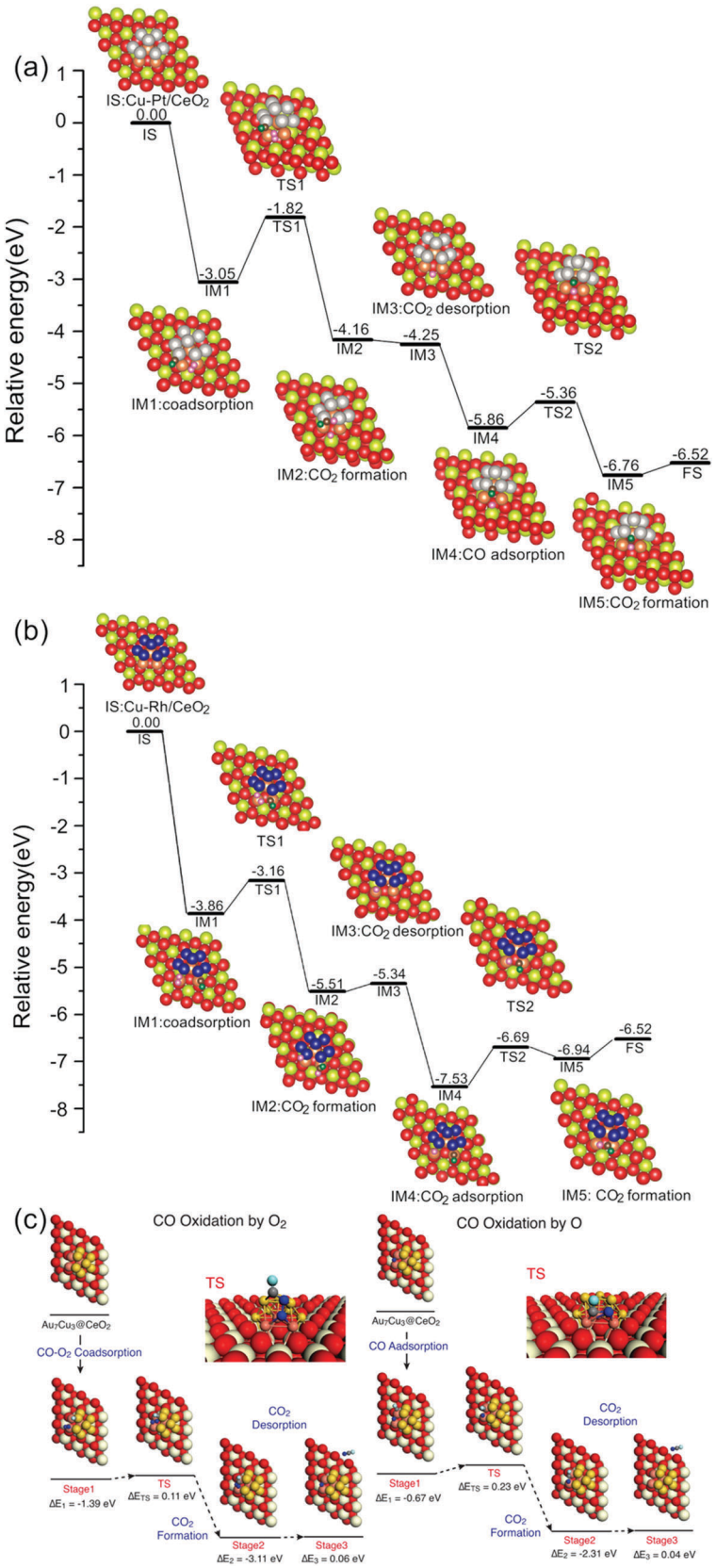

Fig. 3 OCOO mechanisms on CeO_2 supported (a) Cu_3Pt_7, (b) Cu_3Rh_7 and (c) Cu_3Au_7 for CO oxidation. ΔE_x in (c) is the energy of the xth state, relative to the previous stage. In (a and b), red, yellow, orange, silver, blue, pink, grey and green spheres represent oxygen (in ceria), Ce, Cu, Pt, Rh, oxygen (in the gas phase), carbon and oxygen atoms (from CO), respectively. In (c), ivory, red, blue, grey, green, yellow and copper spheres represent Ce, O (CeO_2), O (O_2), C, O (CO), Au and Cu atoms. (c) Reproduced with permission from Zhang *et al.*[37]

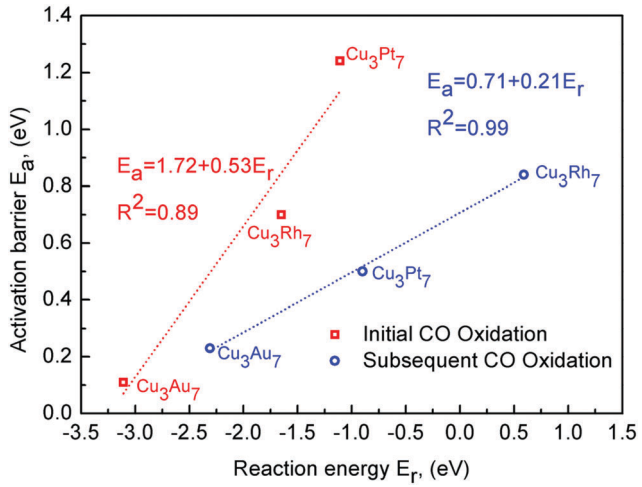

Fig. 4 BEP relationships of the initial and subsequent CO oxidations through the O_2 associative mechanism (OCOO).

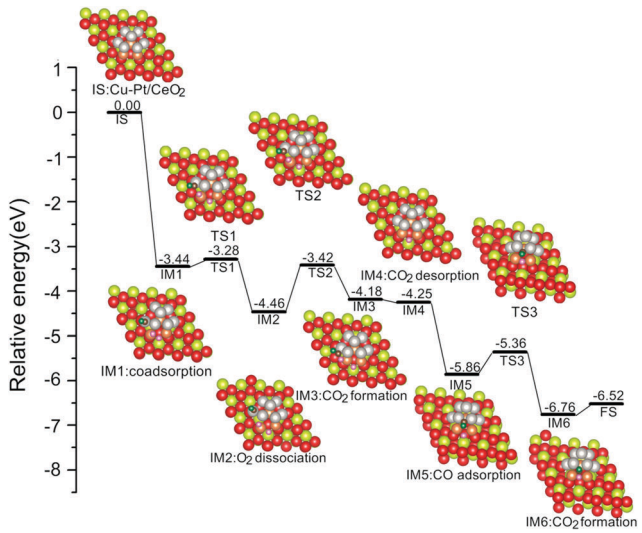

Fig. 5 O_2 dissociation mechanism on the Cu_3Pt_7 system.

here, and keep Cu in a metallic state. Experimental tests would be the best way to determine the stability of such small bimetallic clusters under CO oxidation conditions.

4. Conclusions

In this paper, the bi-functional CO oxidation mechanisms on Cu_3Pt_7 and Cu_3Rh_7 supported on CeO_2(111) were calculated. We found that CO oxidation on Cu_3Pt_7 proceeds by the O_2 dissociation pathway, while Cu_3Rh_7 prefers the OCOO mechanism. Compared with the barriers calculated in a previously-reported study on Cu_3Au_7 supported on CeO_2(111), we found that the theoretical CO oxidation activity of the OCOO mechanism is Cu_3Au_7 > Cu_3Rh_7 > Cu_3Pt_7. A generalized BEP relationship was determined to estimate the key energy barriers of CO oxidation through the O_2 associative pathway (OCOO mechanism). We expect that the mechanistic insights shown in this study could provide a better understanding and guidance for future applications of bi-functional alloy catalysts.

Conflicts of interest

The authors declare no competing financial interest.

Acknowledgements

This work is supported by the Department of Energy under contract DE-FG02-13ER16428 and the Welch Foundation under grant F-1841. The calculations were done at the National Energy Research Scientific Computing Center and the Texas Advanced Computing Center. Yulu Liu thanks the China Scholarship Council for financial support.

References

1 H. J. Freund, G. Meijer, M. Scheffler, R. Schlögl and M. Wolf, *Angew. Chem., Int. Ed.*, 2011, **50**, 10064–10094.
2 W. Song and E. J. M. Hensen, *Catal. Sci. Technol.*, 2013, **3**, 3020–3029.
3 C. Sun, H. Li and L. Chen, *Energy Environ. Sci.*, 2012, **5**, 8475–8505.
4 H. Y. Kim, H. M. Lee and G. Henkelman, *J. Am. Chem. Soc.*, 2012, **134**, 1560–1570.
5 C. Zhang, A. Michaelides and S. J. Jenkins, *Phys. Chem. Chem. Phys.*, 2011, **13**, 22–33.
6 W. J. Zhu, J. Zhang, X. Q. Gong and G. Lu, *Catal. Today*, 2011, **165**, 19–24.
7 M. Haruta, T. Kobayashi, H. Sano and N. Yamada, *Chem. Lett.*, 1987, 405–408.
8 J. Guzman, S. Carrettin and A. Corma, *J. Am. Chem. Soc.*, 2005, **127**, 3286–3287.
9 Y. Lee, G. He, A. J. Akey, R. Si, M. Flytzani-Stephanopoulos and I. P. Herman, *J. Am. Chem. Soc.*, 2011, **133**, 12952–12955.
10 M. Manzoli, F. Boccuzzi, A. Chiorino, F. Vindigni, W. Deng and M. Flytzani-Stephanopoulos, *J. Catal.*, 2007, **245**, 308–315.
11 H. Falsig, B. Hvolbæk, I. S. Kristensen, T. Jiang, T. Bligaard, C. H. Christensen and J. K. Nørskov, *Angew. Chem.*, 2008, **120**, 4913–4917.
12 A. Roldan, J. M. Ricart, F. Illas and G. Pacchioni, *Phys. Chem. Chem. Phys.*, 2010, **12**, 10723–10729.
13 B. Liu, J. Liu, T. Li, Z. Zhao, X. Q. Gong, Y. Chen, A. Duan, G. Jiang and Y. Wei, *J. Phys. Chem. C*, 2015, **119**, 12923–12934.
14 R. Wang, H. He, L. C. Liu, H. X. Dai and Z. Zhao, *Catal. Sci. Technol.*, 2012, **2**, 575–580.
15 M. Jin, J. N. Park, J. K. Shon, J. H. Kim, Z. Li, Y. K. Park and J. M. Kim, *Catal. Today*, 2012, **185**, 183–190.
16 M. J. Lippits, A. C. Gluhoi and B. E. Nieuwenhuys, *Top. Catal.*, 2007, **44**, 159–165.
17 K. Frey, V. Iablokov, G. Melaet, L. Guczi and N. Kruse, *Catal. Lett.*, 2008, **124**, 74–79.

18 A. Alavi, P. Hu, T. Deutsch, P. L. Silvestrelli and J. Hutter, *Phys. Rev. Lett.*, 1998, **80**, 3650–3653.
19 A. D. Allian, K. Takanabe, K. L. Fujdala, X. Hao, T. J. Truex, J. Cai, C. Buda, M. Neurock and E. Iglesia, *J. Am. Chem. Soc.*, 2011, **133**, 4498–4517.
20 M. A. van Spronsen, J. W. M. Frenken and I. M. N. Groot, *Chem. Soc. Rev.*, 2017, **46**, 4347–4374.
21 T. Bunluesin, H. Cordatos and R. J. Gorte, *J. Catal.*, 1995, **157**, 222–226.
22 M. S. Chen, Y. Cai, Z. Yan, K. K. Gath, S. Axnanda and D. W. Goodman, *Surf. Sci.*, 2007, **601**, 5326–5331.
23 W. Liu and M. Flytzani-Stephanopoulos, *Chem. Eng. J.*, 1996, **64**, 283–294.
24 T. J. Huang and D. H. Tsai, *Catal. Lett.*, 2003, **87**, 173–178.
25 B. Eren, C. Heine, H. Bluhm, G. A. Somorjai and M. Salmeron, *J. Am. Chem. Soc.*, 2015, **137**, 11186–11190.
26 P. Kunal, H. Li, B. L. Dewing, L. Zhang, K. Jarvis, G. Henkelman and S. M. Humphrey, *ACS Catal.*, 2016, **6**, 4882–4893.
27 L. Luo, Z. Duan, H. Li, J. Kim, G. Henkelman and R. M. Crooks, *J. Am. Chem. Soc.*, 2017, **139**, 5538–5546.
28 S. Seraj, P. Kunal, H. Li, G. Henkelman, S. M. Humphrey and C. J. Werth, *ACS Catal.*, 2017, **7**, 3268–3276.
29 S. García, L. Zhang, G. W. Piburn, G. Henkelman and S. M. Humphrey, *ACS Nano*, 2014, **8**, 11512–11521.
30 L. D. Sun, M. Hohage, R. Denk and P. Zeppenfeld, *Phys. Rev. B*, 2007, **76**, 245412.
31 X. Lian, P. Xiao, R. Liu and G. Henkelman, *J. Chem. Phys.*, 2017, **146**, 111101.
32 G. Sedmak, S. Hočevar and J. Levec, *J. Catal.*, 2003, **213**, 135–150.
33 X. Liu, A. Wang, X. Wang, C. Y. Mou and T. Zhang, *Chem. Commun.*, 2008, 3187–3189.
34 C. J. Zhang, R. J. Baxter, P. Hu, A. Alavi and M. H. Lee, *J. Chem. Phys.*, 2001, **115**, 5272–5277.
35 S. Lin, X. Ye, R. S. Johnson and H. Guo, *J. Phys. Chem. C*, 2013, **117**, 17319–17326.
36 L. Luo, L. Zhang, Z. Duan, A. S. Lapp, G. Henkelman and R. M. Crooks, *ACS Nano*, 2016, **10**, 8760–8769.
37 L. Zhang, H. Y. Kim and G. Henkelman, *J. Phys. Lett.*, 2013, **4**, 2943–2947.
38 W. Y. Yu, G. M. Mullen, D. W. Flaherty and C. B. Mullins, *J. Am. Chem. Soc.*, 2014, **136**, 11070–11078.
39 E. J. Evans, H. Li, W.-Y. Yu, G. M. Mullen, G. Henkelman and C. B. Mullins, *Phys. Chem. Chem. Phys.*, 2017, **19**, 30578–30589.
40 H. Li and G. Henkelman, *J. Phys. Chem. C*, 2017, **121**, 27504–27510.
41 G. Kresse and J. Furthmüller, *Comput. Mater. Sci.*, 1996, **6**, 15–50.
42 G. Kresse and J. Furthmüller, *Phys. Rev. B: Condens. Matter Mater. Phys.*, 1996, **54**, 11169–11186.
43 S. L. Dudarev, G. A. Botton, S. Y. Savrasov, C. J. Humphreys and A. P. Sutton, *Phys. Rev. B: Condens. Matter Mater. Phys.*, 1998, **57**, 1505–1509.
44 H. Y. Kim and G. Henkelman, *J. Phys. Lett.*, 2013, **4**, 216–221.
45 H. Y. Kim and G. Henkelman, *J. Phys. Lett.*, 2012, **3**, 2194–2199.
46 P. E. Blöchl, *Phys. Rev. B: Condens. Matter Mater. Phys.*, 1994, **50**, 17953–17979.
47 J. P. Perdew, K. Burke and M. Ernzerhof, *Phys. Rev. Lett.*, 1996, **77**, 3865–3868.
48 G. Henkelman, *J. Chem. Phys.*, 2000, **113**, 9901–9904.
49 G. Henkelman and H. Jónsson, *J. Chem. Phys.*, 2000, **113**, 9978–9985.
50 D. C. Sayle, S. A. Maicaneanu and G. W. Watson, *J. Am. Chem. Soc.*, 2002, **124**, 11429–11439.
51 T. X. T. Sayle, S. C. Parker and C. R. A. Catlow, *Surf. Sci.*, 1994, **316**, 329–336.
52 W. Cen, Y. Liu, Z. Wu, H. Wang and X. Weng, *Phys. Chem. Chem. Phys.*, 2012, **14**, 5769–5777.
53 M. Nolan, S. Grigoleit, D. C. Sayle, S. C. Parker and G. W. Watson, *Surf. Sci.*, 2005, **576**, 217–229.
54 C. Zhang, A. Michaelides, D. A. King and S. J. Jenkins, *J. Am. Chem. Soc.*, 2010, **132**, 2175–2182.
55 H. Li, L. Luo, P. Kunal, C. S. Bonifacio, Z. Duan, J. C. Yang, S. M. Humphrey, R. M. Crooks and G. Henkelman, *J. Phys. Chem. C*, 2018, **122**, 2712–2716.
56 N. Dahal, S. García, J. Zhou and S. M. Humphrey, *ACS Nano*, 2012, **6**, 9433–9446.
57 S. D. House, C. S. Bonifacio, J. Timoshenko, P. Kunal, H. Wan, Z. Duan, H. Li, J. C. Yang, A. I. Frenkel, S. M. Humphrey, R. M. Crooks and G. A. Henkelman, *Microsc. Microanal.*, 2017, **23**, 2030–2031.
58 G. W. Piburn, H. Li, P. Kunal, G. Henkelman and S. M. Humphrey, *ChemCatChem*, 2018, **10**, 329–333.
59 K. Shin, L. Zhang, H. An, H. Ha, M. Yoo, H. M. Lee, G. Henkelman and H. Y. Kim, *Nanoscale*, 2017, **9**, 5244–5253.
60 W. Tang, E. Sanville and G. Henkelman, *J. Phys.: Condens. Matter*, 2009, **21**, 084204.
61 K. Mudiyanselage, S. Luo, H. Y. Kim, X. Yang, A. E. Baber, F. M. Hoffmann, S. Senanayake, J. A. Rodriguez, J. G. Chen and P. Liu, *Catal. Today*, 2016, **263**, 4–10.
62 H. Y. Kim and P. Liu, *J. Phys. Chem. C*, 2015, **119**, 22985–22991.
63 A. E. Baber, X. Yang, H. Y. Kim, K. Mudiyanselage, M. Soldemo, J. Weissenrieder, S. D. Senanayake, A. Al-Mahboob, J. T. Sadowski, J. Evans, J. A. Rodriguez, P. Liu, F. M. Hoffmann, J. G. Chen and D. J. Stacchiola, *Angew. Chem., Int. Ed.*, 2014, **53**, 5336–5340.